4Ca^{2+}·Troponin C Forms Dimers in Solution at Neutral pH That Dissociate upon Binding Various Peptides: Small-Angle X-ray Scattering Studies of Peptide-Induced Structural Changes†

S. L. Blechner,‡ G. A. Olah,‡ N. C. J. Strynadka,§ R. S. Hodges,§ and J. Trewhella*,‡

Life Sciences Division, Los Alamos National Laboratory, Los Alamos, New Mexico 87544, and University of Alberta, Edmonton, Alberta, Canada T6G 2H7

Received June 24, 1992; Revised Manuscript Received September 14, 1992

ABSTRACT: Small-angle X-ray scattering data have been measured for rabbit skeletal muscle troponin C and its complexes with the venom peptides melittin and mastoparan as well as synthetic peptides based on regions of the troponin I sequence implicated in troponin C binding. At the neutral pH used in this study (pH 6.8), troponin C shows a tendency to form dimers in the presence of 4 mol equiv of Ca^{2+}, but is monomeric in solution when 2 or less mol equiv of Ca^{2+} is present. The 4Ca^{2+}·troponin C dimers dissociate upon binding melittin, mastoparan, and peptides based on residues 96–115, 1–30, and 1–40 in the troponin I sequence. This result suggests that the peptide-binding sites overlap with the regions of contact between troponin C molecules forming a dimer. Like the structurally homologous calcium-binding protein calmodulin, troponin C shows conformational flexibility upon binding different peptides. Upon binding melittin, troponin C contracts in a similar manner to calmodulin when it binds peptides known to form amphiphilic helices (e.g., melittin, mastoparan, or MLCK-I). In contrast, mastoparan binding to troponin C does not result in a contracted structure. The scattering data indicate troponin C also remains in an extended structure upon binding the inhibitory peptides having the same sequence as residues 96–115 in troponin I.

Troponin C (TnC)[1] is a small (18 kDa) protein that is an integral part of the troponin complex which functions in the calcium-dependent regulation of muscle contraction. TnC is evolutionarily related to calmodulin (CaM) which is involved in the calcium-dependent regulation of a diverse array of biochemical processes. The crystal structures of TnC (Herzberg & James, 1988; Satyshur et al., 1988) and of CaM (Babu et al., 1988) show a strong degree of structural homology. The structures are unusual in that they each consist of 2 globular lobes connected by an extended, solvent-exposed α-helix of 7–9 turns. Each of the globular lobes contains two Ca^{2+}-binding sites which show the characteristic helix–loop–helix motif termed the EF hand (Kretsinger, 1980). Both proteins regulate their respective biochemical processes by binding divalent calcium ions in response to increased local Ca^{2+} concentrations resulting from some physiological stimulus. Ca^{2+} binding in turn induces conformational changes that lead to a change in activity of another protein. In the case of TnC, Ca^{2+} binding to the two low-affinity Ca^{2+}-specific sites in the N-terminal domain results in the release of the inhibitory function of troponin I (TnI) which eventually leads to actin binding to myosin and the triggering of muscle contraction [for a review, see Leavis and Gergely (1984) and Zot and Potter (1987)]. Although the interaction of TnC with the other components of troponin appears to differ in the presence or absence of Ca^{2+}, TnC remains an integral part of the troponin complex in both states. In contrast, CaM more usually binds to its target enzymes only in its Ca^{2+}-saturated form. Ca^{2+} binding to CaM results in the exposure of hydrophobic sites which are thought to facilitate target enzyme binding and activation (Tanaka & Hidaka, 1980; LaPorte et al., 1980). A notable exception to this mode of action for CaM is in phosphorylase kinase (PhK). Like TnC in troponin, CaM remains an integral subunit of this large multicomponent kinase in the presence and absence of Ca^{2+} [for a review, see Picket-Gies and Walsh (1986)].

Small-angle solution scattering has proven a powerful tool for studying the dumbbell-shaped Ca^{2+}-binding proteins because the scattering data are quite sensitive to the relative dispositions of the globular lobes [for a review, see Trewhella (1992)]. Previous small-angle scattering studies of CaM complexed with peptides whose sequences were based on the CaM-binding domains of various target enzymes (Heidorn et al., 1989; Trewhella et al., 1990; Kataoko et al., 1991) and with model peptides (Yoshino et al., 1989; Kataoka et al., 1989) have shown dramatic changes in the relationships between the globular domains, indicating a high degree of structural flexibility in the interconnecting helix. This flexibility appears to be key to CaM's ability to bind to a diverse array of CaM-binding sequences in different target enzymes. We have undertaken similar studies of TnC–peptide complexes in order to see what similarities and/or differences there are between CaM and TnC with respect to their behavior when binding peptides, and hence to gain some understanding of the molecular basis for their functional similarities and differences. We have focused here on studies of the venom peptides melittin and mastoparan known to bind to both CaM and TnC with high affinity and 1:1 stoichiometry, as well as peptides identified in the TnI sequence as TnC-binding domains, including the inhibitory peptide TnI(96–115), and

† This work was performed under the auspices of the U.S. Department of Energy (Contract W-7405-ENG-36) and was supported by NIH Grant GM40528 (J.T.).

* To whom correspondence should be addressed.

‡ Los Alamos National Laboratory.

§ University of Alberta.

[1] Abbreviations: CaM, calmodulin; d_{max}, maximum linear dimension; $\epsilon^{0.1\%}$, extinction coefficient for a 1 mg/mL solution; ϵ^{1mM}, extinction coefficient for a 1 mM solution; MLCK-I, 26-residue CaM-binding peptide corresponding to residues 577–603 in myosin light chain kinase; PhK, phosphorylase kinase; PhK5 and PhK13, 2 25-residue CaM-binding peptides corresponding to residues 342–366 and 302–326 in the catalytic subunit of phosphorylase kinase; R_g, radius of gyration; TnC, troponin C; TnI, troponin I.

0006-2960/92/0431-11326$03.00/0

peptides based on the N-terminal regulatory region, TnI(1–30) and TnI(1–40).

MATERIALS AND METHODS

Sample Preparation. Rabbit skeletal TnC was prepared by the procedure of Chong and Hodges (1982). The purity of the protein was checked by sodium dodecyl sulfate–urea–polyacrylamide gel electrophoresis and isoelectric focusing gel electrophoresis (Chong et al., 1983). The compositions of the synthetic peptides corresponding to residues 1–30, 1–40, and 96–115 of rabbit skeletal TnI were derived from the sequence of Wilkinson and Grand (1978) for rabbit skeletal (fast muscle) TnI. The corresponding peptides synthesized were as follows: TnI(1–30), Ac-GDEEKRNRAITARRQH-LKSVMLQIAATELE-amide; TnI(1–40), NH_2-GDEEKRN-RAITARRQHLKSVMLQIAATELEKEEGRREAEK-amide; TnI(96–115), Ac-NQKLFDLRGKFKRPPLRRVR-amide. Ac corresponds to an acetylated N-terminus and NH_2 to a free amino terminus. All peptides were synthesized on an Applied Biosystems Model 430A peptide synthesizer using the general procedure for solid-phase synthesis described in Parker and Hodges (1985). The crude peptides were purified on a HPLC system using an analytical reverse-phase column [Aquapore-RP-300 (C_8), 220 × 4.6 mm, inner diameter 7 μm, 300 Å; Brownlee Laboratories, Santa Cruz, CA] operated with a linear A/B gradient at a flow rate of 1 mL/min, where solvent A was 0.05% aqueous trifluoroacetic acid and solvent B was 0.05% trifluoroacetic acid in acetonitrile. The gradient rates varied between 0.1% and 0.5% solvent B/min depending on the sample load used (Hodges et al., 1991). Melittin and mastoparan were purchased from Sigma Chemical Company (St. Louis, MO) and purified using the procedure described above.

Protein solutions for scattering experiments were prepared as concentrated (1.67 mM protein) stock solutions by dialyzing against 50 mM MOPS (pH 6.8), 100 mM KCl, 30 mM $CaCl_2$, and 5 mM DTT or alternatively against 100 mM PIPES (pH 6.8), 100 mM KCl, and 5 mM DTT with 0 or 4 mol equiv of $CaCl_2$. With 4 mol equiv of Ca^{2+}, at these TnC concentrations 95% of the TnC has four Ca^{2+} sites occupied, assuming association constants $K_a = 2 \times 10^7$ M^{-1} and 2×10^5 M^{-1} for the high- and low-affinity sites, respectively (Potter & Gergely, 1975). All dilutions of the stock solutions were done by weighing and using buffer solutions taken from the final dialysate. TnC–peptide complexes were prepared with a 10% excess of peptide (i.e., TnC:peptide molar ratio of 1:1.1) to ensure complete complex formation. The TnC–mastoparan complex was also prepared with a 1:2.2 TnC:peptide ratio, since ^{113}Cd NMR data indicate that there may be a second mastoparan-binding site for CaM (Linse et al., 1986). Protein concentrations were determined using a Duram Model D500 amino acid analyzer as described in Pearlstone et al. (1977). The amino acid analyses also provided a check for the correct TnC:peptide stoichiometries. Ca^{2+} concentrations in selected samples were checked by inductively coupled atomic emission spectrometry using a Jarrell-Ash Model 975 ICP AtomComp spectrometer at the Colorado State University Soil Testing Laboratory. Ca^{2+} concentrations quoted are the average of two or three independent measurements on a given sample.

Small-Angle X-ray Scattering Data Acquisition and Analysis. X-ray scattering data were measured using the small-angle instrument described in Heidorn and Trewhella (1988). The sample-to-detector distance was 64 cm. All measurements were taken at room temperature. Detector uniformity was checked after every two series of sample dilution experiments by flooding the position-sensitive linear detector with radiation from an Fe^{55} source.

Scattering data were reduced to $I(Q)$ versus Q for analysis as described in Heidorn and Trewhella (1988). $I(Q)$ is the scattered X-ray intensity per unit solid angle, and Q is the amplitude of the scattering vector. Q is equal to $4\pi \sin \theta/\lambda$, where 2θ is the scattering angle and λ is the wavelength of the scattered X-rays (1.542 Å for the CuKα used). Scattering data were collected for each sample at four to five different protein concentrations in the range of 5–50 mg/mL. The net scattering from the protein molecules was calculated by subtracting a normalized buffer spectrum measured in the same sample cell. Each dilution series was repeated at least once with freshly prepared samples. The effects of interparticle interference were corrected by a linear least-squares extrapolation to zero concentration of the experimental scattering functions divided by the concentration (Pilz, 1982). The extrapolated data thus represent the theoretical scattering from a single particle in solution. Guinier (1939) and the indirect Fourier transform [or $P(r)$] (Moore, 1980) analyses were used to calculate radius of gyration (R_g), forward scatter (I_0), and vector distribution functions [$P(r)$] from the extrapolated data.

R_g for a homogeneous particle is the root-mean-square of the distances of all elemental scattering volumes from the center-of-mass of the particle. Guinier (1939) showed that the intensity of the innermost portion of the scattering profile can be approximated well by a Gaussian curve:

$$I(Q) = I_0 e^{-Q^2 R_g^2/3} \quad (1)$$

For globular objects, the Guinier approximation is typically valid for $QR_g < 1.3$. From eq 1, it can be seen that a plot of ln $[I(Q)]$ vs Q^2 gives a straight line with slope $-R_g^2/3$ and an extrapolated intercept ln I_0.

The pair-distance, or vector distribution function, for a homogeneous scattering particle, $P(r)$, is the frequency of vectors connecting small-volume elements within the entire volume of the scattering particle and is calculated as the inverse Fourier transform of the scattering profile:

$$P(r) = 1/(2\pi^2) \int I(Q) Q \cdot r \sin (Q \cdot r)\, dQ \quad (2)$$

using the indirect Fourier inversion algorithm with slit-smearing, developed by Moore (1980). The vector distribution function goes to zero at a value corresponding to the maximum dimension of the particle, d_{max}. R_g and I_0 can also be calculated from the second and zero moments of $P(r)$, respectively.

The molecular weight, M, of the scattering species is proportional to I_0 at infinite dilution for scattering particles with the same mean scattering density. Using a standard protein of known molecular weight which is monodisperse over a wide range of concentrations, the molecular weight of the scattering particle in another protein sample can be determined simply by taking the ratio of the I_0's:

$$M_{unknown} = (I_{0,unknown}/I_{0,known}) M_{known} \quad (3)$$

Lysozyme was used as the protein standard to determine the molecular weights of the TnC complexes in solution. Lysozyme samples were prepared freshly for each measurement as described in Kringbaum and Kugler (1970). Lysozyme was purchased from the Sigma Chemical Co. and used without further purification.

I_0 for a solution of dimers will be twice that for a solution of monomers, provided the specific volumes of the two forms are equivalent. For a monomer–dimer mixture (Hubbard et

al., 1988), the forward scatter [$I_{0(m-d)}$] can be expressed in terms of I_0 for the monomer [$I_{0(m)}$] and the mole fraction of dimers in the sample, f:

$$I_{0(m-d)} = I_{0(m)}[(3f + 1)/(f + 1)] \quad (4)$$

where f is given by

$$f = c_m/(c_d + c_m) \quad (5)$$

and c_m and c_d are the monomer and dimer molar concentrations, respectively.

Modeling. A modeling procedure was used to find a "best fit" to the experimentally determined $P(r)$ function for the $4Ca^{2+}$·TnC dimer. The initial model for the dimer was based on the crystal structure of TnC (Herzberg & James, 1985) in which only the two high-affinity Ca^{2+}-binding sites in the C-terminal domain were occupied. The crystal structure has two TnC molecules related by a crystallographic symmetry axis, and the N-domain of one molecule interacts with the C-domain of the other molecule via hydrophobic interactions (Strynadka & James, 1990). The α-carbon crystal structure coordinates for the two crystallographically related molecules provided the starting point for the modeling. Models were constructed using homogeneous spheres to represent each amino acid positioned at the crystallographic α-carbon coordinates. The sizes of the spheres were determined from the volume of each amino acid using the values of Jacrot and Zaccai (1981), and the scattering power was determined from the chemical composition. $P(r)$ functions were then calculated using a Monte Carlo integration technique similar to the method described in Heidorn and Trewhella (1988). The model structure was placed in a box, and random points were generated within this box. Points which hit within the molecules were saved, and $P(r)$ functions were calculated from the distances between every pair of saved points. Similar procedures were used to calculate $P(r)$ functions for lower resolution models in which each lobe of a TnC molecule was represented as a uniform scattering density ellipsoid. Ellipsoids were determined by assigning a c-axis in the direction of the longest distance vector between amino acid centers in the lobe with its amplitude equal to half this vector length. Similarly, the a-axis was assigned the direction of the longest distance vector between amino acid centers perpendicular to the c-axis with its amplitude equal to half this vector length, and the b-axis was assigned the direction perpendicular to the a- and c-axes with an amplitude equal to half the vector length of the longest distance vector between amino acid centers which lie in the plane perpendicular to the c-axis and containing the a-axis. The ellipsoids were also increased slightly (2–4 Å in radius) to account for possible hydration layer effects (Zaccai et al., 1986). How possible TnC dimer models were generated from this starting point is described in detail below under Results (see Modeling the Dimer).

Model intensity curves were calculated from the model $P(r)$ functions using the inverse relation of eq 2:

$$I(Q) = 4\pi \int P(r)\,[\sin(Q \cdot r)/(Q \cdot r)]\,dr \quad (6)$$

The corresponding $P(r)$ functions were then recalculated using eq 2 along with the indirect Fourier inversion algorithm over the Q range equivalent to that measured in the experiments. This procedure accounts for truncation effects implicit in the indirect Fourier inversion algorithm arising from the fact that the data can be measured only over a finite Q range.

Intensity curves measured for the $4Ca^{2+}$·TnC samples are a convolution of the particular dimer/monomer population in solution. Using the mole fraction of dimers in MOPS buffer determined using eq 4, and assuming the scattering interference between dimers and monomers to be negligible, the scattering for the dimers alone can be calculated using the relation:

$$I_d(Q) = [I_{m-d}(Q) \cdot (1 + f) - I_m(Q) \cdot (1 - f)]/2f \quad (7)$$

where I_{m-d} and I_m are first scaled appropriately at $Q = 0$ Å^{-1} according to eq 4.

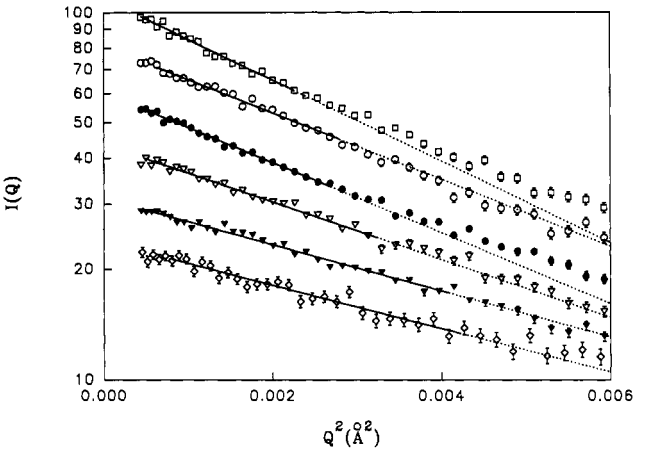

FIGURE 1: Guinier plots of (0–1)Ca^{2+}·TnC (◊) and $4Ca^{2+}$·TnC (○) and of $4Ca^{2+}$·TnC complexed with TnI(1–40) (□), TnI(96–115) (●), mastoparan (▽), and melittin (▼). All of the data shown are for samples in MOPS buffer, except for (0–1)Ca^{2+}·TnC which was in PIPES buffer. Plots have been offset in the y direction for clarity. Solid lines indicate a linear least-squares fit to the data over the Guinier region. Dotted lines are extrapolations of those fits.

RESULTS

Scattering Data. Figure 1 shows Guinier plots calculated for TnC, at infinite dilution, with zero to one and with all four Ca^{2+}-binding sites occupied, as well as for $4Ca^{2+}$·TnC complexed with TnI(96–115), with TnI(1–40), with mastoparan, and with melittin. Each sample measured gives a Guinier region that can be fit with a single straight line with reduced χ^2 values in the range of 0.6–1.4 (Table I). There is no significant upturn at low Q values in the scattering data which would be diagnostic of a large amount of nonspecific aggregation in the samples. TnC and its complexes generally show either no significant concentration dependence of R_g^2 or a linear decrease in R_g^2 with increasing concentration (Figure 2) that can be attributed to interparticle interference effects due to protein–protein repulsion at short distances of approach (Wu & Chen, 1988; Chen & Bededouch, 1986). These observations indicate there is no significant concentration-dependent aggregation in these samples. A notable exception, however, is $4Ca^{2+}$·TnC·melittin in PIPES buffer, which shows a very large increase in R_g (21–28 Å) with increasing protein concentration (10–40 mg/mL). Increases in R_g with increasing protein concentration can be attributed to weak protein–protein attractive forces at short distances of approach (Chen & Bededouch, 1986; Hayter & Zulauf, 1982), although such a large increase is relatively unusual. The concentration dependence, is, however, quite linear, and the value of I_0 extrapolated to infinite dilution (see below) is consistent with that for a single $4Ca^{2+}$·TnC·melittin complex. It is of interest to note that the slope of R_g^2 versus concentration for some of the complexes is quite different for the MOPS- and PIPES-buffered solutions. For example, $4Ca^{2+}$·TnC·melittin in the MOPS-buffered solution shows no concentration dependence. These differences indicate the difference in ionic composition of the buffers is giving rise to

Table I: Structural Parameters from the X-ray Scattering Data on TnC and TnC–Peptide Complexes

	R_g (Å) (Guinier)	χ^2	R_g (Å) [$P(r)$]	d_{max} (Å)	M_r (from I_0)	M_r (sequence)	f
MOPS buffer conditions							
$2Mg^{2+}$·TnC[a]			23.0 ± 0.2	70			
$4Ca^{2+}$·TnC	25.1 ± 0.4	0.9	26.1 ± 0.3	79	33369 ± 2164	17919	0.76 ± 0.13
$4Ca^{2+}$·TnC·melittin	20.8 ± 0.3	1.2	20.7 ± 0.2	68	20096 ± 1350	20986	0
$4Ca^{2+}$·TnC·mastoparan (1:1)	23.2 ± 0.3	1.0	24.1 ± 0.2	73	21332 ± 1000	19545	0.05 ± 0.03
$4Ca^{2+}$·TnC·mastoparan (1:2)	22.5 ± 0.3	1.4	22.9 ± 0.3	72	19727 ± 929	21171	0
$4Ca^{2+}$·TnC·TnI(96–115)	25.7 ± 0.4	0.7	26.0 ± 0.3	76	27783 ± 1072	20693	0.21 ± 0.03
$4Ca^{2+}$·TnC·TnI(1–40)	27.5 ± 0.7	1.0	28.6 ± 0.4	95	26725 ± 1288	23051	0.08 ± 0.03
PIPES buffer conditions							
(0–1)Ca^{2+}·TnC	20.2 ± 0.5	1.0	21.1 ± 0.5	68	17581 ± 1227	17919	0
$2Ca^{2+}$·TnC·TnI(96–115)	21.3 ± 0.5	1.1	22.5 ± 0.4	69	19396 ± 2483	20693	0
$4Ca^{2+}$·TnC	24.9 ± 0.3	1.0	26.9 ± 0.2	73	26915 ± 1177	17919	0.34 ± 0.05
$4Ca^{2+}$·TnC·melittin	18.7 ± 0.2	1.0	19.8 ± 0.4	55	20916 ± 932	20986	0
$4Ca^{2+}$·TnC·mastoparan	22.4 ± 0.3	0.6	23.5 ± 0.2	72	21777 ± 1327	19545	0.06 ± 0.04
$4Ca^{2+}$·TnC·TnI(96–115)	23.5 ± 0.3	0.9	25.2 ± 0.2	72	25255 ± 1120	20693	0.12 ± 0.03
$4Ca^{2+}$·TnC·TnI(1–30)	26.0 ± 0.4	1.3	27.4 ± 0.2	85	23931 ± 947	21722	0.05 ± 0.02

[a] Data from Heidorn and Trewhella (1988).

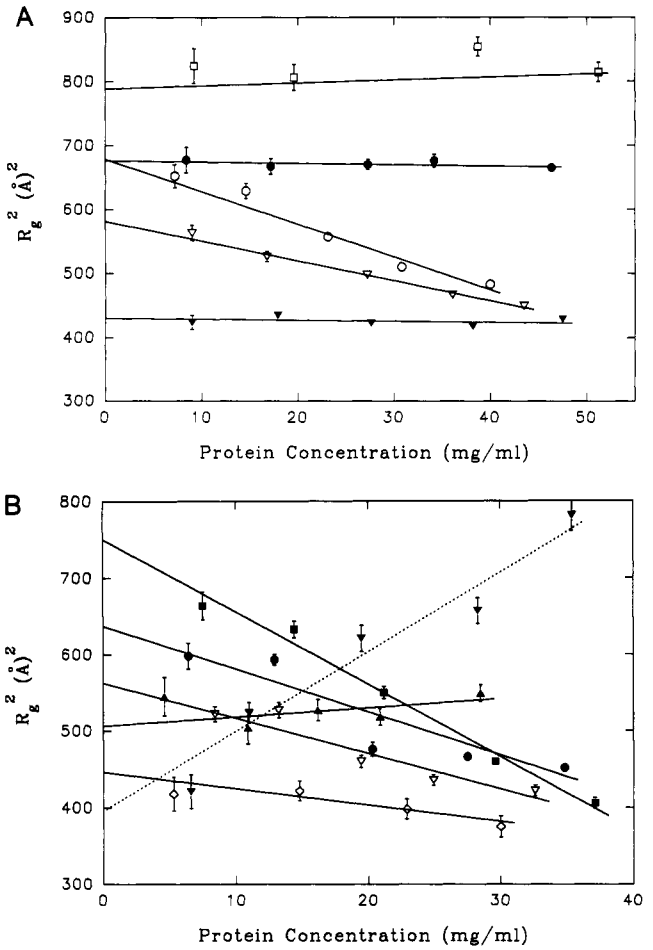

FIGURE 2: R_g^2 versus protein concentration for (0–1)Ca^{2+}·TnC (◇), $2Ca^{2+}$·TnC·TnI(96–115) (▲), and $4Ca^{2+}$·TnC (○) and for $4Ca^{2+}$·TnC complexed with TnI(1–30) (■), TnI(1–40) (□), TnI(96–115) (●), mastoparan (▽), and melittin (▼). (A) Data from samples in MOPS buffer. (B) Data from samples in PIPES buffer.

differences in the interparticle interference effects.

As expected, there is good agreement between the R_g values obtained using the Guinier and the $P(r)$ analyses (Table I) for TnC and for each TnC–peptide complex. I_0 values obtained from the $P(r)$ analysis were used to calculate the molecular weights of the scattering particles for each sample using lysozyme as a standard (Table I). The errors cited include the propagated statistical errors plus uncertainties in the protein concentrations. The molecular weights determined for all $4Ca^{2+}$·TnC samples were consistently larger than that expected for a TnC monomer. In the MOPS-buffered solution (see Materials and Methods), and I_0 value obtained for $4Ca^{2+}$·TnC is close to twice that expected for a TnC monomer, suggesting that the dominant scattering species is a dimer. Using eq 4, and assuming a mixed population of monomers and dimers only, the mole fraction of dimers is calculated as ≈0.76. $4Ca^{2+}$·TnC in the 100 mM PIPES buffer solution gave I_0 values that were smaller than those obtained in the MOPS buffer solutions, but still larger than expected for monodisperse monomers. The mole fraction of dimers is calculated as ≈0.34. Thus, the PIPES buffer solution conditions appear less favorable for dimer formation.

At Ca^{2+} concentrations for which only zero to one of the Ca^{2+}-binding sites of TnC is occupied, the scattering data yield a molecular weight estimate consistent with a single TnC molecule as the scattering particle (Table I). The R_g and d_{max} values obtained under these conditions (in PIPES buffer) are ≈6% smaller than the previously published value for $2Mg^{2+}$·TnC, but the $P(r)$ function (top panel of Figure 3) shows the single maximum at approximately 16 Å and the shoulder at 30–45 Å characteristic of the two-lobed TnC structure with a flexible interconnecting helix region (Heidorn & Trewhella, 1988).

When $4Ca^{2+}$·TnC is complexed with melittin, mastoparan, TnI(1–30), or TnI(1–40), the I_0 data indicate the scattering species is a single TnC–peptide complex (Table I); i.e., binding of these peptides causes the TnC dimers to completely dissociate. In contrast, the I_0 values obtained for the $4Ca^{2+}$·TnC·TnI(96–115) complex in the MOPS or PIPES buffers indicate the TnC dimers are not completely dissociated when the TnI(96–115) peptide binds. The mole fraction of self-associated complexes of $4Ca^{2+}$·TnC·TnI(96–115) in MOPS buffer is ≈0.21, while in PIPES buffer it is ≈0.12. For (0–1)Ca^{2+}·TnC·TnI(96–115), however, the I_0 value indicates the scattering species is a single TnC–peptide complex.

$P(r)$ functions for $4Ca^{2+}$·TnC complexed with melittin and with mastoparan are shown in the middle panel of Figure 3. $4Ca^{2+}$·TnC·melittin gives a $P(r)$ function that indicates a significantly contracted structure compared with (0–1)-Ca^{2+}·TnC. The R_g value for the complex in PIPES buffer is smaller than that measured in MOPS buffer, but in both the MOPS and PIPES buffer solutions, the $P(r)$ functions show a single peak at 23 Å and no evidence for a shoulder at longer vectors, indicating the TnC dumbbell has collapsed into a more globular structure. This conformational change is similar to that seen when CaM binds melittin (Kataoka et al., 1989), mastoparan (Yoshino et al., 1989), the CaM-binding domain

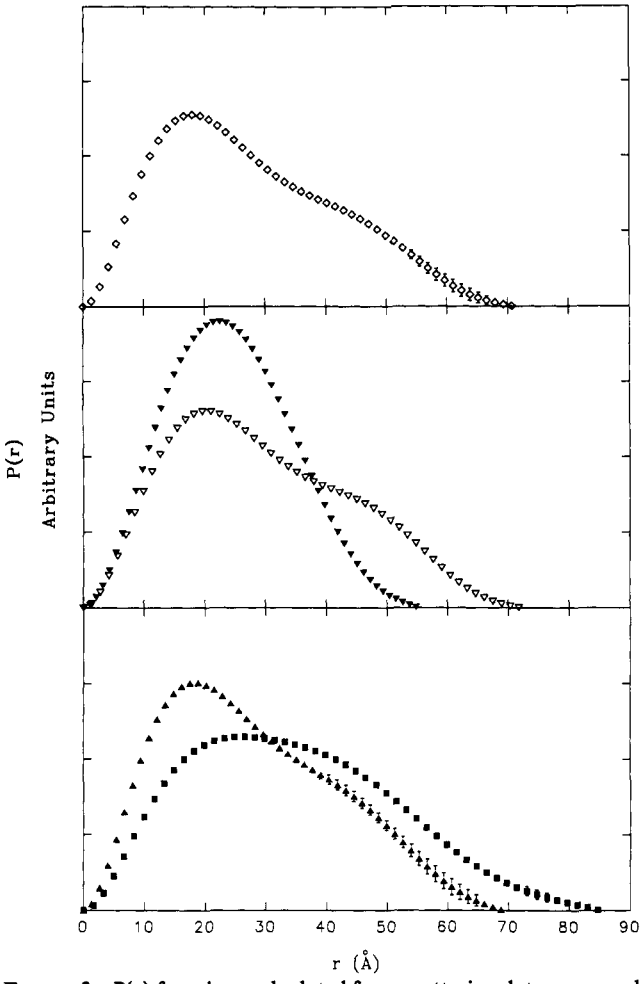

FIGURE 3: $P(r)$ functions calculated from scattering data measured for samples in PIPES buffer: (0–1)Ca^{2+}·TnC (◇); $4Ca^{2+}$·TnC·melittin (▼); $4Ca^{2+}$·mastoparan (▽); $2Ca^{2+}$·TnC·TnI(96–115) (▲); $4Ca^{2+}$·TnC·TnI(1–30) (■). $P(r)$ functions have been put on a relative scale such that the area under each curve is proportional to the molecular weight of the scattering particle.

of myosin light chain kinase (MLCK-I) (Heidorn et al., 1989), or the PhK5 CaM-binding subdomain of the catalytic subunit of PhK (Trewhella et al., 1990). In contrast, the $P(r)$ function for $4Ca^{2+}$·TnC·mastoparan indicates a relatively extended structure like the uncomplexed (0–1)Ca^{2+}·TnC. The R_g value is ≈11% larger than the value obtained for (0–1)Ca^{2+}·TnC (Table I), consistent with the mastoparan binding somewhere away from the center-of-mass of the TnC. The $4Ca^{2+}$·TnC·mastoparan structural parameters are not very different for complexes formed with 1:1.1 and with 1:2.2 TnC:peptide stoichiometries (Table I). Mastoparan is the smallest peptide (M_r 1478) studied, and it is difficult to say definitively whether or not the second mastoparan actually bound since the uncertainties in molecular weights determined from the I_0 data are of the same order as the expected contribution to I_0 from one mastoparan molecule.

The bottom panel of Figure 3 shows the $P(r)$ function for $2Ca^{2+}$·TnC·TnI(96–115). The $P(r)$ function for $2Ca^{2+}$·TnC·TnI(96–115) is very similar to that for (0–1)Ca^{2+}·TnC, indicating that upon binding TnI(96–115) TnC does not undergo any large conformational changes. Similar to $4Ca^{2+}$·TnC, the $P(r)$ functions for $4Ca^{2+}$·TnC·TnI(96–115) (not shown) correspond to the weighted averages for the monomer–dimer mixtures, and the shapes of the $P(r)$ functions were very similar to that observed for $2Ca^{2+}$·TnC·TnI(96–115), with the features all shifted 4–5 Å to longer vector

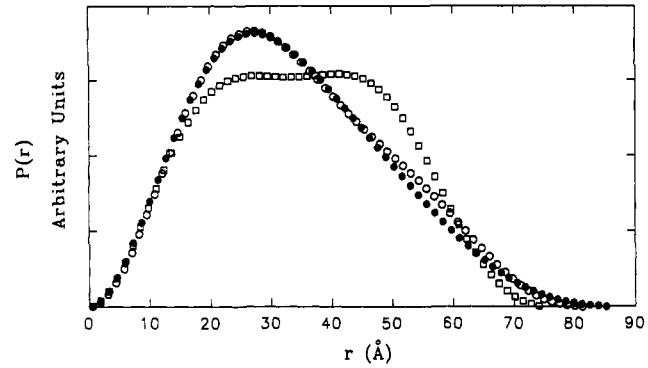

FIGURE 4: $P(r)$ function for the $4Ca^{2+}$·TnC dimer calculated from the scattering data measured in MOPS buffer (○) compared with the dimer derived from the crystal structure (□) and the "best fit" model shown in Figure 5 (●).

lengths. In both the PIPES and MOPS buffers, the $P(r)$ functions for $4Ca^{2+}$·TnC·TnI(96–115) had maximum values at 22 and 24 Å, respectively. These values are 20% and 30% larger than the maximum value for $2Ca^{2+}$·TnC·TnI(96–115).

The bottom panel of Figure 3 also shows the $P(r)$ function for $4Ca^{2+}$·TnC·TnI(1–30) indicating an extended structure for this complex. The TnI(1–30) and TnI(1–40) peptides are the largest of the peptides studied, and it is therefore not surprising that these complexes give the largest R_g and d_{max} values. The complex with TnI(1–30) gives slightly smaller R_g and d_{max} values than the complex with TnI(1–40) (Table I), consistent with the 1–30 peptide being 10 residues shorter. The $P(r)$ functions for both the TnI(1–30) and TnI(1–40) complexes are similar in character except that the maximum for the TnI(1–40) complex at ≈28 Å is a little sharper, and d_{max} is about 10 Å longer.

Experiments were also completed on samples containing approximately equimolar concentrations of $4Ca^{2+}$·TnC, melittin, and TnI(96–115). The scattering data (not shown) were indistinguishable from those obtained for the $4Ca^{2+}$·TnC·melittin complex, including I_0 values, indicating TnI(96–115) does not bind to $4Ca^{2+}$·TnC when melittin is present.

Modeling the Dimer. $P(r)$ for the $4Ca^{2+}$·TnC dimer was calculated using eq 7 from the scattering data measured for the MOPS buffer conditions. $I_m(Q)$ was taken from $2Ca^{2+}$·TnC which is a monomer in solution. The resultant $P(r)$ is shown in Figure 4. The shape of the $P(r)$ function calculated for the $4Ca^{2+}$·TnC dimer in MOPS is similar in character to the $P(r)$ function for the (0–1)Ca^{2+}·TnC monomer, but the features are all shifted to longer vectors; e.g., there is a maximum at 26 Å and a shoulder at ≈45–55 Å. This experimental $P(r)$ does not agree well with the $P(r)$ function calculated from the dimer model based on the crystal structure (Figure 4). The crystal structure dimer gives R_g and d_{max} values that agree with those measured for the dimer, but the $P(r)$ function derived from this model has two pronounced peaks at 22 and 42 Å. The agreement between R_g and d_{max} for the model and experiment suggests that there is something correct in the starting model but that it needs to be modified in some way to give the correct shape for $P(r)$.

Gly-92 in the interconnecting helix of TnC was identified by Herzberg and James (1985) as a point of potential flexibility when they first solved the crystal structure of turkey TnC. Subsequently, we published small-angle X-ray scattering data (Heiborn & Trewhella, 1988) on TnC that indicate the interconnecting helix region is flexible in solution, allowing the globular domains, on average, to be closer together than they are in the crystal structure. Additional models for the

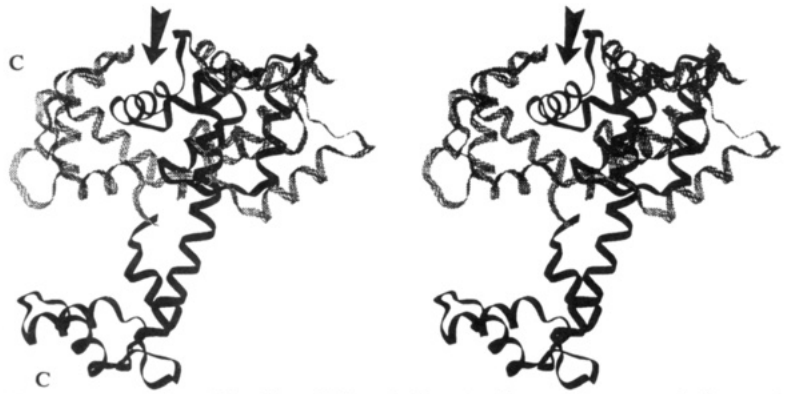

FIGURE 5: Stereoview of a ribbon representation of the "best fit" model for the dimer. The arrow indicates the helix from the N-terminal domain of the one TnC molecule that fits into the hydrophobic cleft of C-terminal domain of the second TnC molecule. The C-terminal domains of each molecule are labeled ("C").

dimer were therefore generated by allowing for flexibility about Gly-92 in each TnC molecule, but maintaining the proximity of the C-terminal domain of the one molecule (TnC1) with the N-terminal domain of the second (TnC2) (Figure 5). Specifically, starting with the atomic coordinates of the original crystal structure, the C-terminal domain of TnC1 was kept rigid, while its N-terminal domain was allowed to rotate randomly about the α-carbon of its Gly-92. The N-terminal domain of TnC2 was then allowed to rotate randomly about its center-of-mass and to translate randomly and only slightly from its original position such that it remained close to TnC1 and preserved some kind of interaction with it. Finally, the C-terminal domain of TnC2 was also allowed to rotate randomly about the α-carbon of its Gly-92. For every random structure generated this way, $P(r)$ functions were calculated, and structures were kept if they gave R_g and d_{max} values within 15% of the measured values, in addition to having the maximum in $P(r)$ at 26 ± 1.5 Å. Among the 25 000 structures generated this way, only 244 structures met these criteria. These 244 structures were inspected using the molecular modeling program INSIGHT (BIOSYM Technologies Inc., San Diego, CA) on a Silicon Graphics workstation (Silicon Graphics Computer Systems, Mountain View, CA). A general feature of these structures was that three of the domains were clustered such that they could potentially interact with each other, while the fourth domain was more distant and surrounded by solvent. Qualitative inspection revealed that structures for which the original hydrophobic interactions were preserved gave $I(Q)$ and $P(r)$ curves that agreed best with the experimental data.

The models generated using the crystal coordinates in the procedure described above contained much higher resolution information than the measured scattering data. All model $P(r)$ functions as a result consistently gave significant differences with the experimental $P(r)$ at short vector lengths. The generated structures were therefore "smeared" by building models that consisted of uniform density ellipsoids constructed to fit the boundaries of each of the four lobes as already described under Materials and Methods. The same Monte Carlo integration technique was used to generate $P(r)$ functions for these lower resolution models. At this resolution, all 244 models fit the short vector lengths in the $P(r)$ function exceptionally well and differed only slightly in peak position (25–28 Å), R_g (25–28 Å), and d_{max} (79–86 Å). The shape of the shoulder on the longer vector length side of the peak varied dramatically for different models. Intensity curves were then calculated for each of the 244 model $P(r)$ functions using eq 5, and a minimum reduced χ^2 analysis was used to find the model intensity curve which best fit the measured data. Reduced χ^2 values for the 244 models varied from 6 to 200. The $P(r)$ function for the model which gave the best fit to the data is compared with the experimental $P(r)$ in Figure 4. This model gives an R_g value of 26.2 Å and a d_{max} of 85 Å.

DISCUSSION

The X-ray scattering data show that $4Ca^{2+}$·TnC has a tendency to form dimers at the neutral pH of 6.8 in the solution conditions used. There is other data to indicate that TnC forms dimers in solution at neutral pH in the presence of Ca^{2+}. Margossian and Stafford (1982) reported a weak Ca^{2+}-induced reversible dimerization ($K_{2,app} = 1.2 \times 10^4$ M^{-1}) of rabbit skeletal TnC based on equilibrium ultracentrifugation. Hubbard et al. (1988) also measured small-angle X-ray scattering data from $4Ca^{2+}$·TnC in the same PIPES buffer conditions that we used, and they report a Ca^{2+}-facilitated dimerization of TnC. However, they calculated a much smaller (<0.075) mole fraction of dimers in their solutions of $4Ca^{2+}$·TnC compared with what we found using the same techniques. This may be attributable to different sample preparation and handling procedures, and/or to the lower protein concentrations (stock solutions of ≈25 mg/mL cf. 40–50 mg/mL) they were able to use because of their more intense X-ray source.

The R_g value and $P(r)$ function determined for the $4Ca^{2+}$·TnC dimers indicate they are relatively compact. Both $2Ca^{2+}$·TnC and $2Mg^{2+}$·TnC are monomeric in solution at pH 6.8, suggesting that the conformational changes associated with Ca^{2+} binding to the two low-affinity sites in TnC result in the exposure of residues which give rise to the intermolecular contacts that form the dimer. Herzberg et al. (1986) presented a model for the Ca^{2+}-induced conformational transition in TnC based on the crystal structure in which only two of the four Ca^{2+}-binding sites are occupied. The model, which has been supported experimentally by several recent site-specific mutations [for a review, see Strynadka and James (1991)], suggests hydrophobic residues in the domain containing the low-affinity Ca^{2+}-binding sites are exposed when helices B and C move away from helices A and D upon Ca^{2+} binding to these sites [helices A–D are labeled in order from the N-terminus according to convention of Herzberg et al. (1986)]. The resulting exposed hydrophobic residues may also facilitate the formation of contacts between $4Ca^{2+}$-TnC molecules. On the basis of the crystal structure of TnC, Strynadka and James (1990) predicted that the major feature of TnC dimerization would involve the interaction of the apolar face of a helix from one TnC molecule into the exposed hydrophobic cleft of a

second TnC molecule with electrostatic interactions being formed by negatively charged groups that surround the hydrophobic cleft. This packing of the helix into the cleft was predicted to mimic the interaction of amphiphilic, helical target peptides with the hydrophobic domains in TnC. It is noteworthy in this regard that the MOPS-buffered solutions favored dimer formation more than the PIPES buffer conditions and that the concentration dependence of R_g^2 is radically different for some of the complexes in the two different buffer solutions, indicating quite different interparticle interference effects. These observations support the proposal that in addition to hydrophobic interactions electrostatic interactions play a role in the dimer formation and that the variations in the ionic composition of the buffer affect these interactions.

Small-angle scattering gives one-dimensional data, and hence it is never possible to prove a single three-dimensional model correct without additional data from another source. However, one can distinguish between classes of model structures, and certain general features can be identified. The general features of having three of the domains in a $4Ca^{2+}$·TnC dimer in close proximity with a fourth somewhat removed and the interaction of the hydrophobic face of a helix of one TnC molecule to the open hydrophobic cleft of a second molecule appear to be such general features.

It is worth noting here that Wang et al. (1989) using solution conditions of 0.1 M KCl/1 mM EDTA did not observe dimerization of skeletal muscle TnC at pH 7.5 in low-speed sedimentation experiments at 20 °C and using polyacrylamide gel electrophoresis under nondenaturing conditions. However, these studies used lower concentrations of TnC than were used for the scattering studies reported here (0.02–0.1 mM compared with 1–2 mM), and since the K_d for the dimerization is only of the order of 10^4 (Margossian & Stafford, 1982), it is not surprising that the dimers are not evident at the lower concentrations. Wang et al. (1989) did observe acid-induced dimerization of rabbit skeletal muscle TnC in the absence of Ca^{2+} in the same set of experiments, and they interpreted their data to indicate that the acid-induced dimerization is also driven by hydrophobic binding. It is interesting to speculate as to whether an acidic environment might induce similar conformational changes in TnC as does Ca^{2+} binding, or if the acid-induced dimer arises from a fundamentally different type of interaction.

The scattering data from the TnC–peptide complexes indicate that, except for TnI(96–115), binding of each peptide results in complete dissociation of the $4Ca^{2+}$·TnC dimers. For $4Ca^{2+}$·TnC·TnI(96–115), the dimers were partially dissociated. These results suggest that there is overlap between the peptide-binding sites and the site of dimerization and are consistent with the fact that the peptides generally have higher affinity for these sites than a second $4Ca^{2+}$·TnC molecule. The fact that TnI(96–115) only partially dissociates the dimers reflects the fact that this peptide has significantly weaker affinity for TnC [$K_{d,TnI(96-115)} = 10^5\ M^{-1}$ (Cachia et al., 1986)] compared with the others [$K_{d,mastoparan} = 5 \times 10^6\ M^{-1}$ (Cachia et al., 1986) and $K_{d,melittin} \gg 10^6\ M^{-1}$ (Steiner & Norris, 1987); K_d's have not been measured for TnI(1–30) or TnI(1–40), but the peptides are assumed to bind with high affinity to TnC in that they remain bound even in the presence of 6 M urea (Ngai & Hodges, 1992)]. In the presence of TnI(96–115) and melittin, I_0 measurements indicate that only the melittin binds to the TnC. The $P(r)$ function is identical to that found for melittin alone, suggesting that the TnI(96–115)-binding site on TnC overlaps with that of melittin and the higher affinity melittin competes for binding with TnI-(96–115).

The venom peptides melittin and mastoparan both have a high propensity to form basic amphiphilic helices with one face of the helix strongly hydrophobic and the opposing face containing polar and positively charged residues. This structural motif has been found to be common to CaM-binding domains in many enzymes regulated by Ca^{2+}–CaM (O'Neil & DeGrado, 1990), including myosin light chain kinase [reviewed in Blumenthal and Krebs (1988)]. In addition, melittin and mastoparan bind with high affinity to CaM, and to TnC, with a 1:1 stoichiometry in a Ca^{2+}-dependent manner. These amphiphilic helices have also been shown to be potent competitive inhibitors of CaM and TnC action. As a result, these peptides have been used in a number of physical studies to model CaM–target enzyme interactions (Blumenthal et al., 1985; Klevit et al., 1985; Klevit & Blumenthal, 1987; Nunnally et al., 1987; Heidorn et al., 1988; Persechini & Kretsinger, 1988a,b; Seeholzer & Wand, 1989; Garone & Steiner, 1990; Ikura et al., 1991, 1992; Roth et al., 1991, 1992). A number of these studies have shown similarities in the interactions of CaM with melittin and mastoparan compared with the CaM-binding domain of myosin light chain kinase, MLCK-I. CD studies (Klevit et al., 1985) indicate a dramatic increase in α-helix content upon CaM binding to MLCK-I, which has also been observed for CaM binding to melittin (Maulet & Cox, 1985) and to mastoparan (McDowell et al., 1985). In addition, small-angle scattering studies have shown that melittin (Kataoka et al., 1989) and mastoparan (Yoshino et al., 1989) induce a similar contraction of CaM as does MLCK-I (Heidorn et al., 1989). This contraction is facilitated by flexibility in the interconnecting helix region of CaM that allows CaM to bring together the two globular lobes, thus encompassing the peptide such that the hydrophobic residues on the peptide helix can interact with both the hydrophobic clefts of the N- and C-terminal domains (Persechini & Kretsinger, 1988a,b; Heidorn et al., 1989; Strynadka & James, 1990; O'Neil & DeGrado, 1989; Ikura et al., 1993). Multidimensional NMR studies support this general model of binding of CaM to MLCK-I, and most recently, Ikura et al. (1993) have presented the NMR solution structure of CaM complexed with MLCK-I detailing specific interactions between the peptide and CaM.

Far-ultraviolet CD measurements also indicate that there is a dramatic increase in helix content when TnC binds melittin or mastoparan compared with the uncomplexed constituents (Cachia et al., 1986). In the case of $4Ca^{2+}$·TnC·melittin, the increased helix content could be entirely attributed to the melittin, but not so for $4Ca^{2+}$·TnC·mastoparan. The scattering data presented here indicate that TnC, like CaM, undergoes a contraction upon binding melittin. The decrease in R_g for $4Ca^{2+}$·TnC·melittin was $\approx$10% compared with $2Mg^{2+}$·TnC in the MOPS buffer conditions, and 14% compared with (0–1)Ca^{2+}·TnC in the PIPES buffer. Furthermore, the $P(r)$ functions for both buffer conditions indicate a contracted shape similar to the CaM·amphiphilic helix type complexes in that the shoulder at long vectors characteristic of the extended dumbbell shapes is not evident and d_{max} is reduced. In contrast to melittin, mastoparan binding does not result in a contracted structure for TnC. Perhaps the significantly shorter mastoparan (14 residues compared to 26 residues in melittin) is not able to make sufficient contacts with both lobes of TnC to stabilize a contracted structure. The interconnecting helix of TnC is somewhat longer than that of CaM which does form

a contracted structure upon binding mastoparan (Yoshino et al., 1989).

Several previous studies have shown that multiple regions of fast skeletal muscle TnI interact with TnC [for a review, see Zot and Potter (1987)]. The TnI peptides studied here encompass the regulatory domain comprised of the N-terminal 40 residues (Ngai & Hodges, 1992) and the inhibitory peptide comprised of residues 104–115 in the TnI sequence. The latter peptide is the minimum sequence required to fully inhibit acto–S1–tropomyosin ATPase activity (Syska et al., 1976; Talbot & Hodges, 1981; Van Eyk & Hodges, 1988). The TnI(96–115) peptide was chosen for the studies here because it includes the inhibitory fragment, but binds with higher affinity to TnC than TnI(104–115). The residues in the inhibitory peptide are predominantly hydrophobic and positively charged, as in the case of mastoparan and melittin. Therefore, it may not be surprising that melittin and the inhibitory peptide share a common binding domain on TnC, thus explaining the apparent displacement of TnI(96–115) by the high-affinity melittin in the scattering study. Several studies have concluded that the TnI inhibitory peptide interacts with regions in the C-terminal domain of TnC [for an overview, see Ngai and Hodges (1992)]. There is also some recent evidence that the inhibitory peptide also interacts with residues in the N-terminal domain (Swenson & Frederickson, 1992; Kobayashi et al., 1991), leading to the speculation that, like calmodulin, TnC may fold over to encompass the sequence TnI(104–115) with both domains simultaneously. However, the solution scattering data presented here indicate no such conformational change in TnC upon addition of the inhibitory peptide.

We have previously suggested that TnC may have an extended structure when complexed with TnI (Trewhella et al., 1990). This prediction was based on scattering data from CaM complexed with the CaM-binding subdomains from the catalytic subunit of phosphorylase kinase, PhK (Dasgupta et al., 1989). Similar to CaM in PhK, TnC is an integral part of the troponin complex and remains so even in the absence of Ca^{2+}. Dasgupta et al. (1989) identified two noncontiguous CaM-binding subdomains in the catalytic subunit of PhK, denoted PhK5 and PhK13, each approximately 25 residues in length. This is quite different than the more typical CaM-binding domain in myosin light chain kinase which is confined to a single smaller region of the sequence ($\approx$18 residues total). PhK5 is predicted to have structural similarities to MLCK-I in having a high propensity for forming an amphiphilic helix. PhK13, however, is predicted to have an extended structure. Further, sequence similarities have been noted between the inhibitory region of TnI. In particular, the highly conserved region corresponding to residues 104–107 in rabbit skeletal TnI is identical to the four N-terminal residues of PhK13 (Dasgupta et al., 1988). These observations led to the suggestion that the interactions between CaM and the catalytic subunit of PhK and between TnC and TnI may be similar. Small-angle scattering data have shown that while CaM contracts upon binding PhK5, the peptide predicted to form a helical structure, it remains extended when it is complexed with PhK13, or with PhK5 + PhK13 (Trewhella et al., 1990). The scattering data from $4Ca^{2+}$·TnC·TnI(96–115) and $2Ca^{2+}$·TnC·TnI(96–115) indicate these complexes have extended structures. These results are in agreement with the TnC fragment studies that show the inhibitory peptide binds to the cleaved C-terminal domain of TnC (Swenson & Frederickson, 1992), and they lend further support to the parallels that have been drawn between the interactions of CaM in PhK and TnC in troponin.

The TnI(1–30) and TnI(1–40) peptides or "regulatory" peptides have recently been shown to bind to TnC with high affinity in a calcium-dependent manner (Ngai & Hodges, 1992). It has been suggested by these authors that this region of TnI may act as a negative regulator of the TnI inhibitory region. Addition of TnI(1–30) and TnI(1–40) to TnC in the presence of calcium prevents the ability of TnC to release TnI(104–115) inhibition of the acto–S1–tropomyosin ATPase activity. This suggests that the regulatory domain and inhibitory domain may share overlapping binding sites on TnC which are alternately occupied by either one or the other at various stages of the contractile event. The solution scattering data presented here indicate that, like TnI(96–115), TnI(1–30) and TnI(1–40) do not induce a major conformational change in TnC but are able to break the dimerization interactions of TnC.

ACKNOWLEDGMENT

We thank Kathy Jones for technical assistance in the preparation of the TnC and TnC–peptide complexes.

REFERENCES

Babu, Y. S., Bugg, C. E., & Cook, W. J. (1988) *J. Mol. Biol. 204*, 191.

Blumenthal, D. K., & Krebs, E. G. (1988) in *Molecular Aspects of Cellular Regulation* (Cohen, P., & Klee, C. B., Eds.) Vol. 5, pp 341–356, Elsevier, Amsterdam.

Blumenthal, D. K., Takio, K., Edelman, A. M., Charbonneau, H., Titani, K., Walsh, K. A., & Krebs, E. G. (1985) *Proc. Natl. Acad. Sci. U.S.A. 82*, 3187.

Cachia, P. J., Van Eyk, J., Ingraham, R. H., McCubbin, W. D., Kay, C. M., & Hodges, R. S. (1986) *Biochemistry 25*, 3553.

Chen, S.-H., & Bededouch, D. (1986) *Methods Enzymol. 130*, 79.

Chong, P. C., & Hodges, R. S. (1982) *J. Biol. Chem. 257*, 2549.

Chong, P. C., Asselbergs, P. C., & Hodges, R. S. (1983) *FEBS Lett. 153*, 372.

Dasgupta, M., Honeycutt, T., & Blumenthal, D. K. (1989) *J. Biol. Chem. 264*, 17156.

Garone, L., & Steiner, R. F. (1990) *Arch. Biochem. Biophys. 276*, 12.

Guinier, A. (1939) *Ann. Phys. (Paris) 12*, 161.

Hayter, J. B., & Zulauf, M. (1982) *Colloid Polym. Sci. 260*, 1023.

Heidorn, D. B., & Trewhella, J. (1988) *Biochemistry 27*, 909.

Heidorn, D. B., Seeger, P. A., Rokop, S. E., Blumenthal, D. K., Means, A. R., Crespi, H., & Trewhella, J. (1989) *Biochemistry 28*, 6757.

Herzberg, O., & James, M. N. G. (1985) *Nature 313*, 653.

Herzberg, O., & James, M. N. G. (1988) *J. Mol. Biol. 203*, 761.

Herzberg, O., Moult, J., & James, M. N. G. (1986) *J. Biol. Chem. 261*, 2638.

Hodges, R. S., Burke, T. W. L., Mant, C. T., & Ngai, S. M. (1991) *High Performance Liquid Chromatography of Peptides and Proteins: Separation, Analysis and Conformation* (Mant, C. T., & Hodges, R. S., Eds.) p 773, CRC Press, Inc., Boca Raton, FL.

Hubbard, S. R., Hodgson, K. O., & Doniach, S. (1988) *J. Biol. Chem. 263*, 4151.

Ikura, M., Kay, L. E., Krinks, M., & Bax, A. (1991) *Biochemistry 30*, 5498.

Ikura, M., Clore, M., Gronenborn, A., Zhu, G., Klee, C. B., & Bax, A. (1993) *Science 256*, 632.

Jacrot, B., & Zaccai, G. (1981) *Biopolymers 20*, 2413.

Katoaka, M., Head, J. F., Seaton, B. A., & Engelman, D. M. (1989) *Proc. Natl. Acad. Sci. U.S.A. 86*, 6944.

Kataoka, M., Head, J. F., Vorherr, T., Krebs, J., & Carafoli, E. (1991) *Biochemistry 30*, 6247.

Klevit, R. E., & Blumenthal, D. K. (1987) in *Proceedings of the 5th International Symposium on Calcium Binding Proteins in Health and Disease*, pp 333–347, Academic Press, New York.
Klevit, R. E., Blumenthal, D. K., Wemmer, D. E., & Krebs, E. G. (1985) *Biochemistry 24*, 8152.
Kobyashi, T., Tao, T., Grabarek, Z., Gergely, J., & Collins, J. H. (1991) *J. Biol. Chem. 266*, 13746.
Kretsinger, R. H. (1980) *CRC Crit. Rev. Biochem. 8*, 119.
Kringbaum, W. R., & Kugler, F. R. (1970) *Biochemistry 9*, 1216.
LaPorte, D. C., Wierman, B. C., & Storm, D. R. (1980) *Biochemistry 19*, 3814.
Leavis, P. C., & Gergely, J. (1984) *CRC Crit. Rev. Biochem. 16*, 235.
Linse, S., Drakenberg, T., & Forsén, S. (1986) *FEBS Lett. 199*, 28.
Margossian, S. S., & Stafford, W. F., III (1982) *J. Biol. Chem. 257*, 1160.
Matsushima, N., Izumi, Y., Matsuo, T., Yoshino, H., Ueki, T., & Miyake, Y. (1989) *J. Biochem. 105*, 883.
Maulet, Y., & Cox, J. A. (1983) *Biochemistry 22*, 5680.
McDowell, L., Sanyal, G., & Prendergast, F. G. (1985) *Biochemistry 24*, 2979.
Moore, P. B. (1980) *J. Appl. Crystallogr. 13*, 168.
Ngai, S.-M., & Hodges, R. S. (1992) *J. Biol. Chem.* (in press).
Nunnally, M. H., Blumenthal, D. K., Krebs, E. G., & Stull, J. T. (1987) *Biochemistry 26*, 5885.
O'Neil, K. T., & DeGrado, W. F. (1989) *Proteins: Struct., Funct., Genet. 6*, 284.
O'Neil, K. T., & DeGrado, W. F. (1990) *Trends Biochem. Sci. 15*, 59.
Parker, J. M. R., & Hodges, R. S. (1985) *J. Protein Chem. 3*, 465.
Paudel, H. K., Carlson, G. M. (1990) *Proc. Natl. Acad. Sci. U.S.A. 87*, 7258.
Pearlstone, J. R., Carpenter, M. R., & Smillie, L. B. (1977) *J. Biol. Chem. 252*, 971.
Persechini, A., & Kretsinger, R. H. (1988a) *J. Biol. Chem. 263*, 12175.
Persechini, A., & Kretsinger, R. H. (1988b) *J. Cardiovasc. Pharmacol. 12 (Suppl. 5)*, S1.
Picket-Gies, C. A., & Walsh, D. A. (1986) *Enzymes (3rd Ed.) 17*, 396–459.
Pilz, I. (1982) in *Small Angle X-ray Scattering* (Glattner, O., & Kratky, O., Eds.) Chapter 8 pp 244–246, Academic Press, New York.
Potter, J. D., & Gergely (1975) *J. Biol. Chem. 250*, 4628.
Roth, S. M., Schneider, D. M., Strobel, L. A., Van Berkum, M. F. A., Means, A. R., & Wand, A. J. (1991) *Biochemistry 30*, 10078.
Roth, S. M., Schneider, D. M., Strobel, L. A., Van Berkum, M. F. A., Means, A. R., & Wand, A. J. (1992) *Biochemistry 31*, 1443.
Satyshur, K. A., Rao, S. T., Pysalska, D., Drendel, W., Greaser, M., & Sundralingham, M. (1988) *J. Biol. Chem. 263*, 1628.
Seeholzer, S. H., & Wand, A. J. (1989) *Biochemistry 28*, 4011.
Steiner & Norris (1987) *Arch. Biochem. Biophys. 254*, 342.
Strynadka, N. C. J., & James, M. N. G. (1990) *Proteins: Struct., Funct., Genet. 7*, 234.
Strynadka, N. C. J., & James, M. N. G. (1991) *Curr. Opin. Struct. Biol. 1*, 905.
Swenson & Frederickson (1992) *Biochemistry 31*, 3420.
Syska, H., Wilkinson, J. M., Grand, J. A., & Perry, S. V. (1976) *Biochem. J. 153*, 375.
Talbot, J. A., & Hodges, R. S. (1981) *J. Biol. Chem. 256*, 2798.
Tanaka, T., & Hidaka, H. (1980) *J. Biol. Chem. 255*, 11078.
Trewhella, J. (1992) *Cell Calcium 13*, 407.
Trewhella, J., Blumenthal, D. K., Rokop, S. E., & Seeger, P. A. (1990) *Biochemistry 29*, 9316.
Van Eyk, J. E., & Hodges, R. S. (1988) *J. Biol. Chem. 236*, 1726.
Wang, C. K., Lebowitz, J., & Cheung, H. C. (1989) *Proteins: Struct., Funct., Genet. 6*, 429.
Wilkenson, J. M., & Grand, R. J. M. (1978) *Nature 271*, 31.
Wu, C.-F., & Chen, S.-H. (1988) *Biopolymers 27*, 1065.
Yoshino, H., Minari, O., Matsushima, N., Ueki, T., Miyake, Y., Matsuo, T., & Izumi, Y. (1989) *J. Biol. Chem. 264*, 19706.
Zaccai, G., Wachtel, E., & Eisenberg, H. (1986) *J. Mol. Biol. 190*, 97.
Zot, A. S., & Potter, J. D. (1987) *Annu. Rev. Biophys. Biophys. Chem. 16*, 535.

Registry No. Melittin, 20449-79-0; mastoparan, 72093-21-1.